

Effects of Superhyperfine Interactions on Photon-Echo Behavior in Dilute Ruby*†

L. Q. Lambert

Department of Physics, University of Chicago, Chicago, Illinois 60637

(Received 23 August 1972)

A detailed analysis of the photon-echo decay in dilute ruby is presented. The experimental results are in quantitative agreement with an echo-decay theory based on the magnetic interaction between the Cr electronic spin and neighboring Al nuclear magnetic moments. Specifically, the following photon-echo properties are explained by the Cr-Al interaction: (i) modulation of the echo as a function of pulse separation time, (ii) the rapid decay of the echo from the ${}^4A_2(m_s=3/2)$ to ${}^2E(m_s=1/2)$ transition, (iii) the dependence of the echo on the direction and magnitude of an external magnetic field, (iv) the echo behavior at the 2.06- and 4.12-kG level crossings, and (v) the photon-echo decay in low magnetic fields. In addition, the experiments presented here show that the Cr-Al magnetic interactions in the 2E excited state are roughly the same as the corresponding interactions in the 4A_2 ground state. The relationship of the photon-echo results to recent fluorescence-linewidth measurements is discussed.

I. INTRODUCTION

In a recent paper, Compaan¹ reported studies of the Cr concentration-dependent decay of the photon echo in ruby. Compaan described the loss of phase memory resulting from random fluctuations of the local magnetic fields in the ruby crystal. In one model, these magnetic fluctuations are due to random spin flips of neighboring Cr ions and thus give a concentration-dependent decay. With the additional assumption of random statistical distribution of Cr ions, the theory predicts, and Compaan's experiments confirm, the nonexponential character of photon-echo decay in ruby.

There are, however, many aspects of the photon-echo decay in ruby which are not concentration dependent. In this paper we explore one such decay process due to Al nuclei which are near neighbors of the laser-excited ions. The Al neighbors and the Cr ion form a magnetically coupled multilevel system from which the decay arises from interference of coherent states. This process is physically quite different from the photon-echo decay studied by Compaan, inasmuch as the Cr-Al decay does not result from the irreversible loss of phase memory but rather from the interference of different radiation modes.² There are cases for Cr-Al interactions where the *apparent* loss of phase memory is actually the result of interference and the echo signal is recoverable. Since much of the basic theory of photon echoes³⁻⁵ and the theory of photon-echo and spin-echo decay and modulation^{6,7} has been treated by other authors, only a general, concise approach to the theory is presented, in terms of which a large body of photon-echo data presented here for the first time is analyzed.

The early experiments on photon echoes in ruby revealed a number of physical properties of the echo which were not explained in terms of the simple theory³ of photon echoes based on a two-level

system. For example, the first experiments showed that it was necessary to apply a magnetic field along the optic axis of the crystal in order to observe an echo.^{3,8} Early experiments also measured the decrease in echo intensity as the magnetic field was tilted with respect to the optic axis.^{3,9} Other work showed that there is a time-dependent modulation of the photon echo for off-axis magnetic fields.¹⁰ All of these echo phenomena are the result of the fact that the superposition states of the Cr ion in ruby (the 4A_2 ground state and the 2E excited state) actually consist of a multiplet of energy levels due to the interaction of the Cr spin with neighboring Al nuclear magnetic moments. In a previous paper² which analyzed the effects of nearly degenerate states on photon-echo behavior, it was shown that both the fluorescence and echoes from coherently excited multilevel systems exhibit time-dependent modulations of intensity. Basically this modulation occurs whenever an atom is coherently excited to a state which consists of a superposition of nearly degenerate energy levels. Each of these levels radiates at a slightly different frequency, which gives rise to an interference in the radiation from a *single atom*. Modulated fluorescence has been discussed in the literature¹¹ and has been observed in experiments using beam-foil excitation,¹² pulsed electron-beam excitation,¹³ and weak pulsed optical excitation.¹⁴ A comparable example of interference from coherent states in a quite different area of physics is the decay of the K^0 meson.¹⁵ We shall show in this paper that the observed modulation of photon-echo intensity in ruby and related effects are further examples of the self-interference in the radiation from coherently excited multilevel systems. The photon-echo modulations discussed here differ from those of our previous paper² insofar as the source of the coherent superposition of states is different. Here the coupling of different levels within the ground- or excited-state multiplets oc-

curs indirectly as the result of the interaction of the Cr spin with neighboring Al nuclear moments, and not coupling via the radiation field itself. This indirect coupling requires a somewhat different formalism. A detailed theoretical treatment of the photon-echo modulation due to the Cr-Al interaction in ruby has been given by Grischkowsky and Hartmann,⁸ and is formally quite similar to the spin-echo modulation theory of Rowan, Hahn, and Mims.⁷ In this paper we give a compact presentation of the Cr-Al modulation theory used in the analysis of our experimental data.

Early photon-echo experiments in ruby,^{3,8-10} were performed using linearly polarized laser pulses. This unfortunately precluded any detailed analysis based on the spin-dependent Cr-Al interaction, since the relative contributions of different Cr spin states were unknown. The first observation of circularly polarized echoes was reported by Compaan, Lambert, and Abella.¹⁶ In this paper, extensive new data taken with circularly polarized laser pulses in dilute ruby, mostly in 0.006 wt% of Cr₂O₃ in Al₂O₃, are presented. Using these new data we shall show that many of the observed properties of the photon echo are the result of the Cr-Al interaction and are in quantitative agreement with the theory. Specifically, the following photon-echo properties are explained: (i) the modulation of the echo as a function of pulse separation time,¹⁰ (ii) the rapid decay of the echo arising from the ⁴A(*m_s* = ³/₂) to ²E(*m_s* = ¹/₂) transition,¹⁰ (iii) the dependence of the echo on the direction and magnitude of an external magnetic field, (iv) the behavior¹⁶ of the echo at the 2.06- and 4.12-kG level crossings, and (v) the photon-echo decay in low magnetic fields. Furthermore, a best-fit analysis has been made of the data on echo intensity versus angle of magnetic field (relative to the optic axis) to determine some of the excited-state interaction parameters which have not been directly measured. Preliminary estimates of excited-state interaction parameters have been made both by ourselves¹⁶ and others.⁶ In both cases the analysis failed to include the effect of the Al nuclear quadrupole moment and consequently led to somewhat erroneous conclusions. Some comments shall also be made on the relationship of the data to recent experiments on laser-induced-fluorescence line narrowing in ruby.¹⁷ However, we should note that this paper deals only with photon-echo phenomena related to the Cr-Al interaction and does not treat echo properties related to the magnetic interaction of Cr spins with other Cr spins such as the concentration-dependent echo decay.¹

II. THEORY

In this section a brief discussion is given of the theory of fluorescence and photon echoes from multilevel systems of nearly degenerate states. The

basic theory of fluorescence and photon echoes from multilevel systems has been developed in a recent paper by Lambert, Compaan, and Abella,² which extended the work of Gordon *et al.*⁵ Here the theory is specialized to treat the more complex problem encountered with photon echoes in ruby. The equations we obtain describing the effect of the interaction of the Cr spin and the Al nuclei on the echo intensity are in most respects equivalent to the equations of Grischkowsky and Hartmann⁶ who approach the problem from a different point of view. Our approach yields additional information on the effect of the variation of optical transition matrix elements not shown in earlier treatments. These matrix-element effects are crucial for accurate analysis of the data. The theory presented here shows that modulated fluorescence and photon-echo modulation in ruby have similar origins.

The radiation from an optical system excited by short intense pulses of coherent radiation can be described by calculating the expectation value of the electric dipole moment using the familiar density-matrix approach. We start with the equation given by Lambert *et al.*² for the electric dipole moment of a single atom, evaluated in a reference frame "rotating" at the frequency of the incident radiation field:

$$\begin{aligned} \langle \vec{P} \rangle &= \text{Tr}[\vec{P}\rho(t)] \\ &= \text{Tr}[\vec{P} e^{-i\mathcal{H}t/\hbar} e^{i\vec{F}\cdot\vec{P}} \rho(0) e^{-i\vec{F}\cdot\vec{P}} e^{i\mathcal{H}t/\hbar}], \end{aligned} \quad (1)$$

where \mathcal{H} is the effective Hamiltonian in the "rotating frame" and $\vec{F} = \int_0^{\Delta\tau} dt \vec{\mathcal{E}}(t)/\hbar$, where $\Delta\tau$ is the pulse width and the incident electric field of the pulse is given by $\vec{\mathcal{E}}(t) = \vec{\mathcal{E}}(t) \cos\omega t$. The initial density matrix $\rho(0)$ characterizes a quasi-two-level system having sets of ground states $\{|a\rangle\}$ and excited states $\{|b\rangle\}$ which consist of two (or more) nondegenerate levels. During the time the incident laser field is present, we have neglected all terms in the Hamiltonian except the interaction with the electric field $\vec{F}\cdot\vec{P}$; this is valid for those ions whose resonant frequency is very near the central frequency of the laser pulse, i. e., well within the linewidth of the laser. There are, of course, other ions farther off resonance which contribute to the radiation for which the above resonance approximation is not valid; however, this approximation affects the absolute amplitude of the radiation but not the essential phase-coherence properties. For off-resonant ions the excitation cannot be simply represented by the $e^{i\vec{F}\cdot\vec{P}}$ terms; however, phase coherence is determined primarily by the $e^{i\mathcal{H}t/\hbar}$ terms which have the same form on or off resonance. So as far as coherence properties are concerned, we lose nothing by retaining the resonance assumption.

As shown in the paper of Lambert *et al.*² the nonzero terms of the trace are

$$\langle \vec{P} \rangle = \frac{1}{2} \sum_{ab} \langle a | \vec{P} | b \rangle \langle b | e^{-i\mathcal{H}t/\hbar} | b \rangle \times \langle b | \sin(2\vec{F} \cdot \vec{P}) | a \rangle \langle a | e^{i\mathcal{H}t/\hbar} | a \rangle + c. c. \quad (2)$$

Here we have written the equation in a form which is more convenient for the calculation in the case of ruby. We now specialize to the ruby crystal where the multiplicity of ground and excited states is due to the interaction of the Cr spin with neighboring Al nuclear magnetic moments. The state of the coupled system of the Cr ion and Al nuclei can be represented by a state function for the Cr ion multiplied by a state function for the nuclear spins. Thus we can write the states $|a\rangle$ and $|b\rangle$ as the direct product of a state vector representing the Cr and a state vector representing the Al neighbors,

$$\begin{aligned} |a\rangle &= |\alpha\rangle |\{m_j\}\rangle, \\ |b\rangle &= |\beta\rangle |\{n_j\}\rangle, \end{aligned} \quad (3)$$

where $|\alpha\rangle$ represents one of the four 4A_2 ground states, $|\beta\rangle$ one of the two 2E excited states, and $\{m_j\}$ and $\{n_j\}$ are sets of quantum numbers for the spins of the Al neighbors j . The electric dipole operator \vec{P} operates only on the Cr-ion part of the state function so when Eqs. (3) are substituted into Eq. (2), we obtain

$$\begin{aligned} \langle \vec{P} \rangle &= \frac{1}{2} \sum_{\alpha\beta} \langle \alpha | \vec{P} | \beta \rangle \langle \beta | \sin(2\vec{F} \cdot \vec{P}) | \alpha \rangle \\ &\times \left(\sum_{\{m\}\{n\}} \langle \{m_j\} | \{n_j\} \rangle \langle \{n_j\} | e^{-i\mathcal{H}t/\hbar} | \{n_j\} \rangle \right. \\ &\left. \times \langle \{n_j\} | \{m_j\} \rangle \langle \{m_j\} | e^{i\mathcal{H}t/\hbar} | \{m_j\} \rangle \right). \quad (4) \end{aligned}$$

Here $\mathcal{H}_\alpha = \langle \alpha | \mathcal{H} | \alpha \rangle$ and $\mathcal{H}_\beta = \langle \beta | \mathcal{H} | \beta \rangle$ are Hamiltonians corresponding to the 4A_2 and 2E states, respectively, and are given explicitly by Eqs. (9). We define a transformation matrix W whose elements are $\langle \{n_j\} | \{m_j\} \rangle$; this matrix transforms Al eigenstates for the 4A_2 state to the Al eigenstates for the 2E state. Rewritten in terms of the matrix W , the electric dipole moment becomes

$$\langle \vec{P} \rangle = \frac{1}{2} \sum_{\alpha\beta} \langle \alpha | \vec{P} | \beta \rangle \langle \beta | \sin(2\vec{F} \cdot \vec{P}) | \alpha \rangle \times [\text{Tr}(W^\dagger e^{-iE_\beta t/\hbar} W e^{iE_\alpha t/\hbar})]. \quad (5)$$

Here E_α and E_β are the diagonal operators representing the Hamiltonians \mathcal{H}_α and \mathcal{H}_β . The radiation intensity is obtained by transforming the electric dipole moment back into the laboratory reference frame, squaring and taking the average over times long compared to the optical frequencies. Assuming that only one of possible $|\alpha\rangle$ to $|\beta\rangle$ transitions is resonant, the intensity is

$$I \sim |\langle \alpha | \vec{P} | \beta \rangle \langle \beta | \sin(2\vec{F} \cdot \vec{P}) | \alpha \rangle|^2$$

$$\times |\text{Tr}(W^\dagger e^{-iE_\beta t/\hbar} W e^{iE_\alpha t/\hbar})|^2. \quad (6)$$

This equation which we evaluate later predicts modulations in the fluorescence from a ruby crystal which is coherently excited by a laser pulse.

This predicted fluorescence modulation is intimately related to the photon-echo modulation which has been observed in ruby, as we shall now show by calculating the photon-echo intensity versus pulse separation. For a sequence of two pulses we retain only those terms which contribute to the echo at $t = 2\tau$. Following Ref. 2 we obtain for the electric dipole moment $\langle \vec{P} \rangle$ in the rotating frame:

$$\begin{aligned} \langle \vec{P} \rangle &= \frac{1}{2} \sum_{a'a''bb'} \langle a | \vec{P} | b \rangle \langle b | e^{-i\mathcal{H}(t-\tau)/\hbar} | b \rangle \\ &\times \langle b | \sin(\vec{F}_2 \cdot \vec{P}) | a' \rangle \langle a' | e^{-i\mathcal{H}\tau/\hbar} | a' \rangle \\ &\times \langle a' | \sin(2\vec{F}_1 \cdot \vec{P}) | b' \rangle \langle b' | e^{i\mathcal{H}\tau/\hbar} | b' \rangle \\ &\times \langle b' | \sin(\vec{F}_2 \cdot \vec{P}) | a \rangle \langle a | e^{i\mathcal{H}(t-\tau)/\hbar} | a \rangle + c. c., \quad (7) \end{aligned}$$

where τ is the pulse separation time.

If we again specialize to ruby by making the substitutions for $|a\rangle$ and $|b\rangle$, and assume only one of the $|a\rangle$ to $|b\rangle$ transitions is resonant, the result in terms of the matrix W is

$$\begin{aligned} \langle \vec{P} \rangle &= \frac{1}{2} \langle \alpha | \vec{P} | \beta \rangle [\langle \beta | \sin(\vec{F}_2 \cdot \vec{P}) | \alpha \rangle]^2 \\ &\times \langle \alpha | \sin(2\vec{F}_1 \cdot \vec{P}) | \beta \rangle \\ &\times [\text{Tr}(W^\dagger e^{-iE_\beta(t-\tau)/\hbar} W e^{-iE_\alpha\tau/\hbar} \\ &\times W^\dagger e^{iE_\beta\tau/\hbar} W e^{iE_\alpha(t-\tau)/\hbar})] + c. c. \quad (8) \end{aligned}$$

For ruby the ground- and excited-state Hamiltonians^{18,19} are given explicitly by

$$\begin{aligned} \mathcal{H}_\alpha &= g_\alpha \mu_B \vec{S} \cdot \vec{H} + D[S_x^2 - \frac{1}{3}S(S+1)] + \mathcal{H}_{A1}, \\ \mathcal{H}_\beta &= \delta + g_\beta \mu_B S_x H_x + \mathcal{H}_{A1}, \end{aligned} \quad (9)$$

where g_α and g_β are the 4A_2 and 2E state g factors, μ_B is the Bohr magneton, \vec{S} is the electron spin operator, \vec{H} is the external magnetic field, D is the quadrupole splitting of the 4A_2 ground state, and δ represents the optical energy shift due to inhomogeneities in the crystal field. The interaction with neighboring Al nuclear magnetic moments is treated as a perturbation, in which we make the "effective-field" approximation, i. e., the Cr spin is viewed as a source of an external magnetic field for the Al nuclei. The Hamiltonians for the Al nuclei can then be written as

$$\begin{aligned} \mathcal{H}_{A1} &= \sum_j \{ \vec{I}_j \cdot [-\mu_n \vec{H} + A_j \langle \vec{S} \rangle] \\ &+ B_j (3\vec{r}_j \langle \vec{S} \rangle \cdot \vec{r}_j - r_j^2 \langle \vec{S} \rangle) / r_j^5 \} \\ &+ Q_j [I_x^2 - \frac{1}{3}I(I+1)], \quad (10) \end{aligned}$$

where \vec{I}_j is the nuclear spin operator for Al neigh-

bor j , μ_n is the nuclear magnetic dipole moment, A is the strength of the contact interaction, B is the strength of the magnetic-dipole interaction, \vec{r}_j is the position vector of the Al relative to the Cr site, and Q is the electric quadrupole splitting. The interaction parameters A , B , and Q and the expectation value of the spin (\vec{S}) are evaluated for either the 4A_2 or 2E state as appropriate. The effective magnetic fields are calculated using the expectation value of the Cr spin. The operator \mathcal{H}_{A_1} evaluated for the 4A_2 state does not commute with the same operator evaluated for the 2E state since the expectation value for the Cr spin will be different for the ground and excited states. Since these Hamiltonians do not commute, pulsed excitation creates a superposition of nuclear eigenstates.

The condition that the energy-level separation be within the linewidth of the laser ensures that the Cr spin state will be uniquely determined for both the 4A_2 ground state and the 2E excited state for all ions contributing to the echo. Consequently, each diagonal Hamiltonian (E_α or E_β) in Eq. (8) can be written simply as the sum of a scalar quantity representing the energy of the Cr ion and a Hamiltonian for the Al nuclei; the scalar terms cancel leaving only the noncommuting Al Hamiltonians.

If we neglect the small magnetic-dipole interaction between the Al nuclei, they can be treated independently, i. e., the Hamiltonian for one Al nucleus commutes with the Hamiltonian for any other nucleus. Equation (8) can then be factored into a product with each factor representing the effect of a particular Al site. For each Al neighbor j , we diagonalize the corresponding term in Eq. (10) to obtain the diagonal representation of the 4A_2 ground- and 2E excited-state nuclear-spin Hamiltonians $E_{\alpha,j}$ and $E_{\beta,j}$. From the nuclear-spin eigenvectors obtained in the above diagonalization a transformation W_j can be determined which transforms from ground-state eigenvectors to excited-state eigenvectors. Thus for $t = 2\tau$ the trace in Eq. (8) can be rewritten as

$$\langle \vec{P}(2\tau) \rangle \sim \prod_j \text{Tr} (W_j^\dagger e^{-iE_{\beta,j}\tau/\hbar} W_j e^{-iE_{\alpha,j}\tau/\hbar} \times W_j^\dagger e^{iE_{\beta,j}\tau/\hbar} W_j e^{iE_{\alpha,j}\tau/\hbar}). \quad (11)$$

Here the transformations W_j are related to the transformation W of Eq. (8) by a direct product $W = \prod_j W_j$. The trace in Eq. (11) is taken over the six eigenstates ($\frac{5}{2}$ spin) of the individual Al nuclei. In practice the echo is calculated from Eq. (11) by doing a numerical diagonalization to determine $E_{\alpha,j}$, $E_{\beta,j}$, and W_j from the Hamiltonians given by Eq. (10). We used the standard IBM subroutine HDIAG to do the numerical diagonalization. The parameters A_j , B_j , and Q_j are known for the 4A_2 ground state from the ENDOR data of Laurance, McIrvine, and Lambe,¹⁹ while the corresponding

parameters for the 2E excited state have not been previously determined experimentally. The excited-state parameters are treated as adjustable parameters in the theory. We wish to point out that Eq. (11) is equivalent to the results for Grischkowsky and Hartmann,⁶ however, the scalar factors given by the terms containing $|\alpha\rangle$ and $|\beta\rangle$ in Eq. (8) do not appear in their treatment. These terms as we shall show in Sec. IV, where we compare theory and experiment for echoes, are very important in calculating the echo versus the angle of magnetic field.

In the case of fluorescence following a single laser pulse, substitution of the explicit Hamiltonians for ruby into Eq. (6) gives an echo intensity proportional to

$$I \sim \left| \prod_j \text{Tr} (W_j^\dagger e^{-iE_{\beta,j}t/\hbar} W_j e^{iE_{\alpha,j}t/\hbar}) \right|^2. \quad (12)$$

Evaluation of this equation typically gives a modulation of the fluorescent intensity when a magnetic field is applied to the sample.

III. EXPERIMENTAL APPARATUS

The photon echo in ruby is generated by irradiating a liquid-He-cooled ruby sample with two sequential laser pulses produced by a liquid-N₂-temperature ruby laser. Figure 1 is a schematic of the experimental apparatus used in the experiments described in this paper. The pulse from the laser is divided by a beam splitter with one portion focused immediately on the 1.0-mm-thick sample of ruby 0.006 wt% Cr. The other portion is sent through a variable-optical-delay line (White cell)²⁰ consisting of a pair of 1.5-m confocal spherical mirrors, before being focused to the same point on the sample. As previously reported,^{1,10} this variable-delay line can be used to make direct measurements of photon-echo decay. The generation of circularly polarized photon echoes requires the circularly polarized laser pulses to propagate parallel to the optic axis of the crystal while the magnetic field applied to the sample must be aligned within a few degrees of the optic axis. To satisfy both of these requirements, we used a 0° sample and two small mirrors between the pole faces of the magnet to direct the beam along the axis of the sample. The beam incident on the first small mirror was linearly polarized in the plane of incidence so that the linear polarization was preserved after reflection. The laser pulse was then converted to circular polarization by a mica quarter-wave plate placed over the quartz window of the sample Dewar. Another quarter-wave plate was used to convert back to linear polarization in the detection end. The echo is spatially and temporally resolved from the incident pulses with an aperture and Kerr-cell arrangement. The echo is

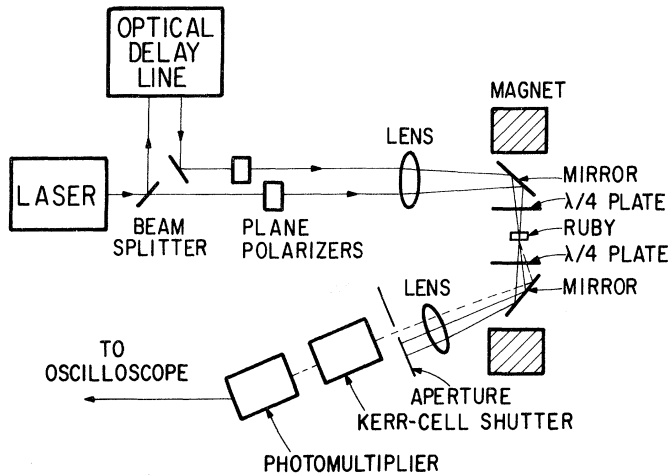


FIG. 1. Experimental arrangement for the observation of circularly polarized photon echoes.

detected by a photomultiplier and displayed on a Tektronix 585-A oscilloscope. The liquid-He-cooled sample is centered between the pole faces of a rotatable 6-in. Varian electromagnet capable of producing a 6-kG field at the sample. The experimental arrangement allows the magnet to be rotated through approximately 36° about the vertical axis. The He Dewar also can be tilted $\pm 3^\circ$ about a horizontal axis which is perpendicular to the direction of the laser beam. This allows the optic axis of the ruby crystal to be accurately aligned with the magnetic field.

An important feature of the apparatus used in these experiments is the use of a tunable ruby laser. The physical construction of the laser is identical to the laser described in Ref. 3. This laser is made tunable by the addition of an external pump and pressure regulator to control the N_2 vapor pressure above the liquid- N_2 reservoir, thus controlling its temperature. The need for tuning capability can be illustrated from Fig. 2 which shows the familiar energy-level diagram for ruby,¹⁸ with the possible circularly polarized laser transitions ${}^4A_2(m = \pm \frac{3}{2}) \rightarrow {}^2E(\bar{E})(m = \pm \frac{1}{2})$ and ${}^4A_2(m = \pm \frac{1}{2}) \rightarrow {}^2E(\bar{E})(m = \pm \frac{1}{2})$ designated by $\sigma_1(+\frac{3}{2} \rightarrow +\frac{1}{2})$, $\sigma_2(-\frac{1}{2} \rightarrow -\frac{1}{2})$, $\sigma_3(+\frac{1}{2} \rightarrow +\frac{1}{2})$, and $\sigma_4(-\frac{3}{2} \rightarrow -\frac{1}{2})$, which is in the order of increasing energy at high field. The σ_1 and σ_4 transitions in the N_2 -cooled laser (77°K) overlap the σ_2 and σ_3 transitions in the He-cooled sample. The σ_2 and σ_3 transitions can easily be made resonant with the laser over the entire 6-kG range of magnetic field available, since the Zeeman shift is due only to the difference in the g factor between the ground ($g = 1.98$) and excited states ($g = 2.44$). Cooling the laser below 77°K increases its frequency thus tuning it off the σ_2 and σ_3 transitions in the sample; the σ_1 transition can then be brought into resonance for magnetic fields in the region between 1 and 3 kG. The use of thermal tuning of the laser and circularly polarized incident pulses

allows the σ_1 , σ_2 , and σ_3 transitions to be studied independently. This in turn makes it possible to study the spin dependence of the photon-echo decay, particularly the details near the 2- and 4-kG level crossings.

IV. EXPERIMENTAL RESULTS

As stated in Sec. I, all early photon-echo experiments in dilute ruby were done with linearly polarized laser pulses. Two recent papers have presented photon-echo data from circular-polarization experiments in ruby. In one paper¹⁶ it was shown experimentally that the photon-echo decay in ruby depends on the spin state of the Cr ion.

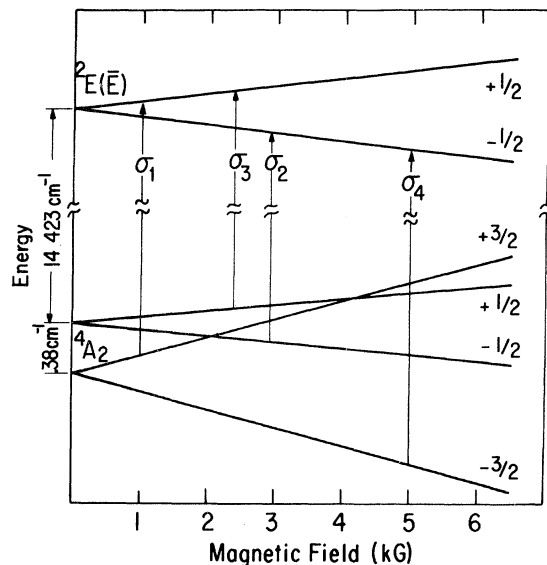


FIG. 2. Energy levels for the 4A_2 to ${}^2E(\bar{E})$ transitions in ruby for a magnetic field parallel to the optic axis, $\theta = 0$. The four circularly polarized transitions are designated in the order of increasing energy at high fields: $\sigma_1(+\frac{3}{2} \rightarrow +\frac{1}{2})$, $\sigma_2(-\frac{1}{2} \rightarrow -\frac{1}{2})$, $\sigma_3(+\frac{1}{2} \rightarrow +\frac{1}{2})$, and $\sigma_4(-\frac{3}{2} \rightarrow -\frac{1}{2})$.

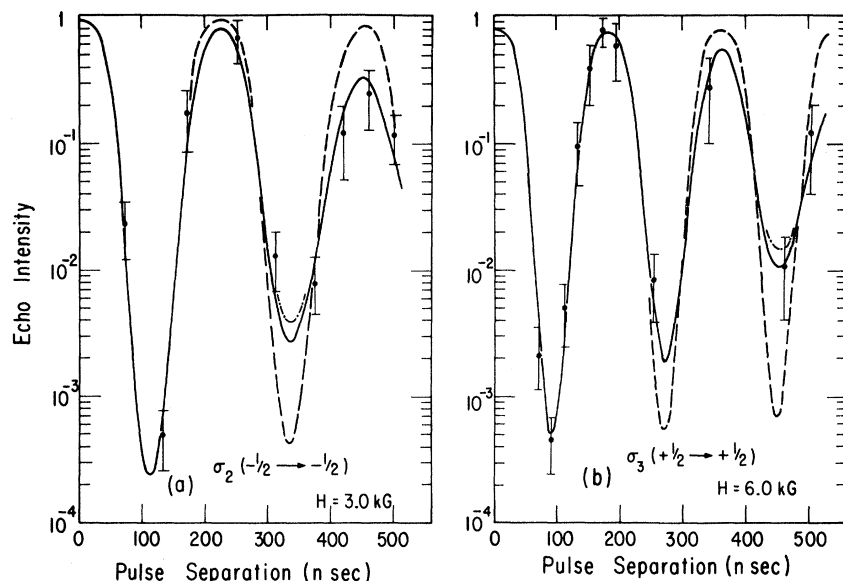


FIG. 3. Photon-echo intensity as a function of pulse separation time: (a) for the $\sigma_2(-\frac{1}{2} \rightarrow -\frac{1}{2})$ transition for a 3.0-kG field at $\theta = 8^\circ$ to optic axis, and (b) for the $\sigma_3(+\frac{1}{2} \rightarrow +\frac{1}{2})$ transition for 6.0 kG at $\theta = 5^\circ$. Points shown were taken from echo-vs-magnetic-field-angle data by assuming no echo modulation for fields parallel to the optic axis. The solid curves are the theoretically predicted modulations. The dashed curves show the effect of neglecting the nuclear electric quadrupole moment in the calculation. The curve with the dash-dotted sequence is the result of using remeasured quadrupole parameters of Ref. 21 in the region most sensitive to the quadrupole moments.

This paper showed clearly that it was necessary to use circularly polarized laser pulses in order to adequately investigate photon echoes in ruby. Another recent paper by Compaan¹ has reported the concentration-dependent photon-echo decay in ruby using circular polarization. In this paper extensive new data are presented for dilute ruby 0.006 wt% Cr, taken with circularly polarized laser pulses. Specifically, data on the modulation of the echo as a function of pulse separation time, the dependence of the echo on the angle of an external magnetic field, and the echo at the level crossings are presented. Using these data the concentration-independent properties of the photon-echo decay are investigated and are shown to be due to the interaction of the Cr spin with neighboring Al nuclear magnetic moments.

A. Echo Modulation and Magnetic Field Dependence

The modulations of the photon echo are predicted by the theory presented in Sec. II. In Eq. (11) the echo is expressed as a function of the eigenfrequencies of the Al nuclei. When an external magnetic field of a few kilogauss is applied to the ruby sample, the frequencies of all 13 nearest Al neighbors are about the same. In the presence of such a magnetic field the modulation effects of all the Al neighbors are essentially in phase; this results in a strong modulation of the echo for the σ_2 and σ_3 transitions as shown in Fig. 3. Figure 3(a) shows experimental data and a theoretical curve (solid line) for the echo intensity versus pulse separation time for the σ_2 transition for a magnetic field of 3 kG at an angle of 8° to the optic axis. Figure 3(b) shows the σ_3 transition for a 6-kG field 5° off axis. The theoretical curves were computed from Eq.

(11) with the Hamiltonians of Eq. (10) using the 4A_2 ground-state interaction parameters of Laurance, McIrvine, and Lambe.¹⁹ The 2E parameters for the contact and quadrupole interactions were assumed to be the same as the ground-state parameters while the dipole contribution was scaled in proportion to the excited-state g factor. The 4A_2 ground-state parameters have been redetermined²¹ recently. However, these new values differ from those of Laurance *et al.*¹⁹ by only a few percent except for two of the quadrupole parameters, and we do not expect these new values to change the photon-echo calculations significantly (see Fig. 3).

For both the σ_2 and σ_3 transitions the depth of the modulation increases as the angle of the magnetic field is increased with respect to the optic axis as indicated by the angular dependence data in Figs. 4 and 5. In fact, for the on-axis fields used in our experiments, the theory predicts a modulation of at most 20% of the echo signal for the σ_2 transition and 10% for the σ_3 transition which is too small to be observed experimentally with our apparatus. The absence of any significant on-axis modulation was confirmed by previously published data on the direct measurement of photon-echo decay.^{1,10} With direct echo versus pulse separation measurements the off-axis modulation appears superimposed on a slower continuous decay which is observed both on and off axis. This slow continuous decay in low-concentration ruby arises in part from the Cr-Cr interaction discussed by Compaan¹ and, perhaps, in part from farther Al neighbors or simply systematic experimental error. This component of the decay will not be analyzed in this paper. The modulation effect can be separated from the con-

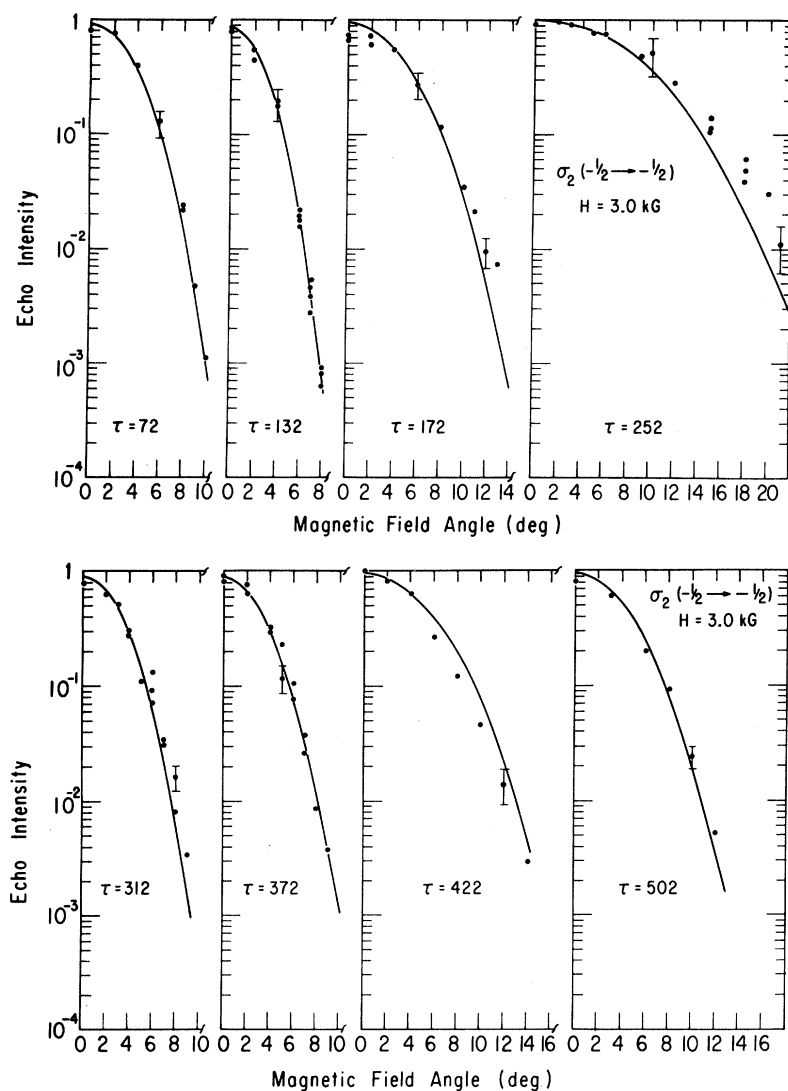


FIG. 4. Photon-echo intensity observed as a function of the angle of the magnetic field with respect to the optic axis. The data are for the $\sigma_2(-\frac{1}{2} \rightarrow -\frac{1}{2})$ transition with a field of 3.0 kG for various pulse separation times. Curves are computed from theory as discussed in text.

tinuous decay by taking a series of angular dependence curves for different pulse separations and assuming that the on-axis modulation is negligible. The data points in Fig. 3 were obtained in this way from the angular dependence data of Figs. 4 and 5.

The solid curves in Figs. 4 and 5 were computed from the theory by taking the excited-state contact and quadrupole parameters to be the same as the ground-state parameters. For the σ_2 transition the angular dependence data at 3 kG are in excellent agreement with the theory as shown in Fig. 4. For the σ_3 transition at 6 kG the agreement between theory and experiment is quite good for angles less than 8° , but some discrepancies occur at larger angles (Fig. 5). The discrepancies may arise from the fact that the optical-transition energy is a function of the angle of the magnetic field. Thus changing the angle of the magnetic field can tune the sample on or off resonance with

the laser. This shift in optical-transition energy is sufficient to account for the errors in the σ_3 angular dependence; however, the exact resonance conditions were not measured for these experiments. The optical resonance for the σ_2 transition at 3 kG is not significantly changed by the angle of the magnetic field, which is probably the reason for better agreement in the σ_2 case.

The quantitative details of the angular dependence are rather complicated but the physical explanation is quite simple. For on-axis magnetic fields the ground- and excited-state electron spins are aligned along the optic axis of the crystal, thus for the σ_2 and σ_3 transitions there is very little change in the magnetic field at the Al sites, hence there is little change in the Al state. This implies that for each ground-state energy level, excitation occurs predominantly to a single excited-state level; thus effectively approximating a two-level system for

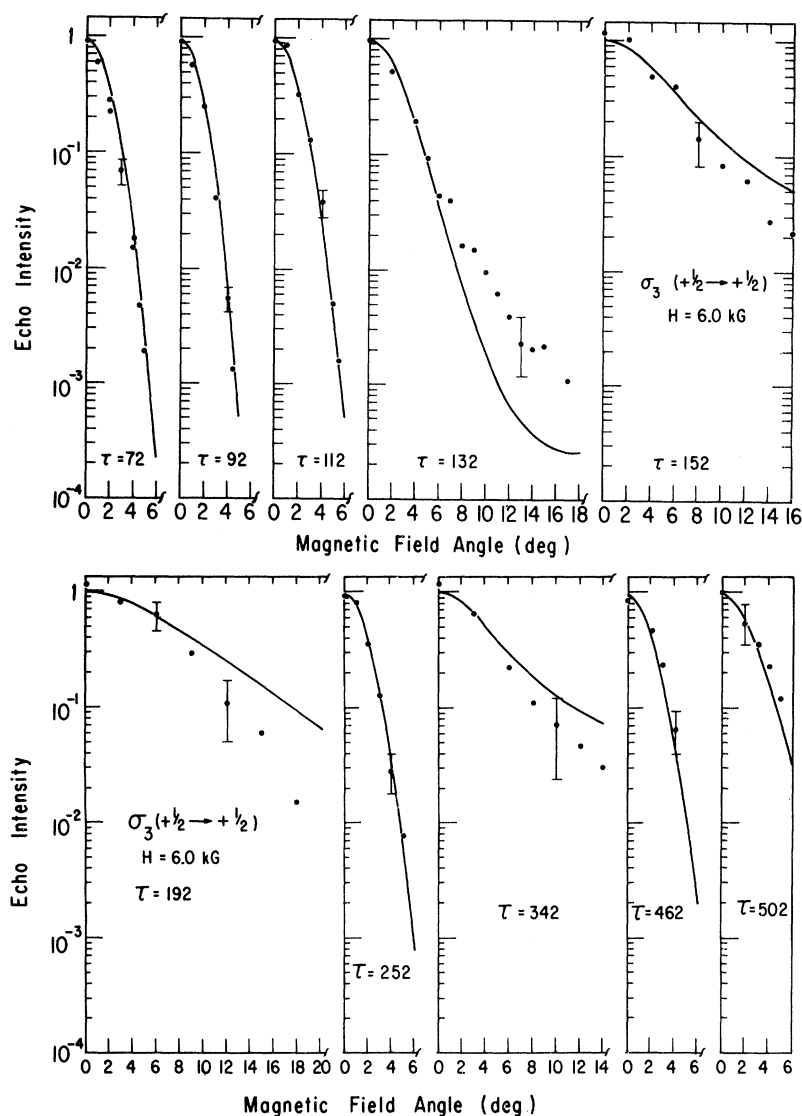


FIG. 5. Photon-echo intensity observed as a function of the angle of the magnetic field with respect to the optic axis. The data are for the $\sigma_3(+\frac{1}{2} \rightarrow +\frac{1}{2})$ transition with a field of 6.0 kG for various pulse separation times. Curves are computed from theory as discussed in the text.

which there is no interference in the subsequent radiation. Mathematically, the transformations W_i in Eq. (11) are very nearly identity matrices in this case. As the magnetic field is tilted away from the optic axis the excited-state spins remain aligned with the optic axis whereas the ground-state spins are aligned in different directions which can be determined by diagonalizing the ground-state Hamiltonian, Eq. (9). It is this difference in Cr spin orientation between the ground and excited states which gives rise to the angular dependence of the modulation.

The effect of the nuclear electric quadrupole moment can be understood by first considering the case where there is no quadrupole moment. Then the energy levels for each Al nucleus are evenly spaced which gives a very limited number of modulation (difference) frequencies. Introducing the

quadrupole splitting produces an uneven spacing of the nuclear energy levels, hence a greater number of modulation frequencies and a "washing out" of the modulation. This is shown by comparing the dashed curves (no Q moment) and the solid curves (with Q moment) of Fig. 3. The quadrupole terms in the Al Hamiltonians are particularly important at longer pulse separation times and at large magnetic field angles. Neglecting these terms has previously led to the misinterpretation of experimental data,^{6,16} which are discussed in detail below.

In addition to the angular dependence of the modulation, there is a *time-independent* angular dependence due to the variation of the transition matrix element. The scalar factors consisting of the terms containing $|\alpha\rangle$ and $|\beta\rangle$ in Eq. (8) show that the echo amplitude is proportional to the fourth power of the electric dipole matrix element.

For off-axis magnetic fields the ground-state energy levels are represented by linear combinations of the Cr spin states oriented along the optic axis. As an example consider the σ_2 transition from a ground-state energy level with a spin function containing the term $C|-\frac{1}{2}\rangle$, where $|C|^2 \leq 1$; the contribution to the photon-echo intensity from this level will be proportional to C to the eighth power. In Figs. 4 and 5 both the angular dependence of the modulation and the angular dependence of the matrix elements are included in the calculation of the theoretical curves, in fact both are necessary to get a good fit to the data. The angular dependence of the matrix element is itself a function of the transition and the magnetic field. For example, the echo for σ_2 at 3 kG and 18° is reduced to 56.5% of the intensity at 0° , while the echo for σ_3 at 6 kG and 18° is reduced to 11.6%. The fact that the modulation curves of Fig. 3 do not go to unity at $\tau=0$ is a result of the matrix-element variation.

B. Excited-State Parameters

We have thus far presented calculations which assume the excited-state contact and quadrupole interactions have the same strength as the corresponding ground-state interactions. However, it is possible to vary the strengths of the excited-state interactions to give a best fit to the data. We have used the angular dependence data of Figs. 4 and 5 to determine the excited-state interaction parameters for the 13 nearest Al neighbors. These 13 neighbors consist of a single nearest neighbor on the optic axis and four sets of three axially symmetric neighbors.¹⁹ There are, thus, five independent parameters for the strength of the contact interaction and five for the quadrupole interaction. In the experiments presented here, only the relative echo intensities are experimentally significant; the absolute intensities vary from one experiment to another in an uncontrollable manner. Therefore, in fitting the data we compare theoretical and experimental intensity ratios, e.g., the ratio of the echo intensity for some fixed angle of magnetic field to the echo intensity for an on-axis field. Furthermore, the primary source of error in the data are random fluctuations in the echo intensity. These fluctuations are roughly proportional to the echo intensity. The nature of the data implies that we should make a logarithmic fit to the data; namely, we wish to minimize the quantity $\sum_i (\ln I_i - \ln \Phi_i)^2$, where I_i is a theoretical intensity ratio and Φ_i the corresponding experimental ratio. The best way to fit the angular dependence data would be to do a least-squares fit to all the angular dependence data points. This approach, however, would require computing several hundred points for each trial choice of parameters and would be prohibitively time consuming. We have

chosen to fit a restricted set of data in order to make the problem manageable. Those data for each angular dependence curve (Figs. 4 and 5) consist of the ratio of the echo intensity at the largest angle of magnetic field for which a reliable intensity can be measured to the echo intensity for the on-axis field. These ratios were taken for 19 angular dependence curves for different fixed pulse separations including data for both σ_2 and σ_3 transitions. The range of pulse separations is from 72 to 502 nsec. As a first approximation the data fitting was done assuming the quadrupole parameters are the same in the excited state and the ground state. This is a reasonable approximation, since the ground-state quadrupole splittings¹⁹ of the 12 off-axis Al neighbors differ from the quadrupole splitting²² of an Al nucleus in pure Al_2O_3 by 3–22%. This indicates that the presence of the Cr ion is a second-order effect on the nuclear quadrupole splitting. Thus we expect that the excited-state quadrupole parameters will not be significantly different from those in the ground state. The problem is now reduced to determining five contact interaction parameters. The results of this least-squares analysis indicate that the various Al sites affect the echo in different proportions. The single-ion on-axis was found to have essentially no effect on the echo, i. e., never more than a 3% change in echo intensity. For the other sites the best choices for the ratio of the excited-state contact interaction to the ground-state contact interaction were $R(I)=0.9$, $R(J)=1.0$, $R(K)=1.0$, and $R(L)=0.7$, where the indices I, J, K, L are the site designations of Laurance *et al.*¹⁹ The parameter used to characterize the goodness of the logarithmic fit is the root-mean-square deviation of experimental and theoretical points. When the contact interaction ratios are all chosen to be 1.0, the rms deviation is 0.87. Choosing $R(I)=0.9$ reduces this quantity by 11% whereas choosing $R(L)=0.7$ reduces it by only 1%. Since the statistical error in each datum point is typically 30–50%, the departures from a value of $R=1.0$ for the best-fitted parameters are not believed to be experimentally significant.

Grischkowsky and Hartmann⁶ have previously analyzed early photon-echo angular dependence data of Abella *et al.*³ taken with linearly polarized laser pulses, using substantially the same theoretical approach as presented here. However, these authors neglected to include several important factors in their analysis. First, they do not include the angular dependence due to matrix-element variation. They also assumed in their analysis that the effects of the nuclear quadrupole interaction were negligible, which we point out is important for either large angles or longer pulse separation times. The angular dependence curves

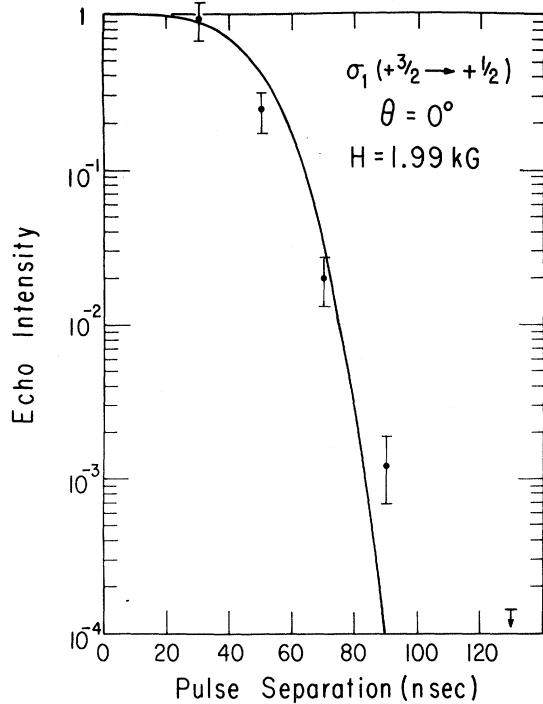


FIG. 6. Photon-echo decay for the $\sigma_1(+\frac{3}{2} \rightarrow +\frac{1}{2})$ transition with a magnetic field of 1.99 kG parallel to the optic axis. The data are from Ref. 16 and the curve from our theory.

for the early data have been recalculated including the quadrupole moments and the matrix-element effect. The data for the 50-nsec pulse separation can be fitted very well by assuming equal contributions of the σ_2 and σ_3 transitions and a contact interaction ratio of 1.0 for all Al neighbors. The data for $\tau = 100$ nsec do not fit the equal contribution curve quite as well; however, all data points lie between the σ_2 and σ_3 angular dependence curves for a contact ratio of 1.0. Thus, our results appear to be consistent with the early data.

C. Decay of $\sigma_1(\frac{3}{2} \rightarrow \frac{1}{2})$ Echo

In addition to the σ_2 and σ_3 transitions, we have reported¹⁶ experimental observation of the decay of the photon echo from the σ_1 transition. The photon-echo intensity versus pulse separation for this transition is shown in Fig. 6 for a magnetic field parallel to the optic axis. The experimental observations for the σ_1 transition are qualitatively quite different from the σ_2 and σ_3 transitions insofar as no modulation is observed but rather a continuous and rapid decay. The theoretical curve in Fig. 6 computed from Cr-Al interaction is in substantial agreement with the data, which further confirms our analysis. The rapid decay in this case is due to the large change in magnitude of the Cr spin during the optical transition. b-

served echo at longer pulse separation time may contain a contribution from the σ_2 transition which has the same circular polarization.

D. Level Crossings

From the three transitions discussed, it is clear that the echo decay depends strongly on the change in the expectation value of the Cr spin due to the optical excitation. The echo can thus be viewed as a probe of the Cr spin state. When the 4A_2 ground state is near a level crossing where there is considerable mixing of spin states, the photon-echo decay is observably affected. The properties of the photon echo due to the spin behavior of the Cr near the 2-kG level crossing have been discussed in an earlier paper.¹⁶ The calculations in that paper did not include nuclear-quadrupole effects discussed here. In Fig. 7 we present the theoretical fit obtained at the 2-kG level crossing by including the quadrupole moment. As above, the quadrupole and contact interaction parameters are assumed to be the same for the ground and excited states. The peak in the echo signal for the σ_1 transition is due to the fact that the expectation value of the Cr spin near the level-crossing field is $+\frac{1}{2}$ for both resonant energy levels. For the σ_2 transition at the level crossing, the excitation effectively occurs from a $+\frac{1}{2}$ spin state to a $-\frac{1}{2}$ spin state which produces a large change in magnetic field at the Al sites.

The level crossing at 4 kG affects the echo in the σ_3 transition as shown by the new data presented in Fig. 8. With the exception of the background signal of 4×10^{-3} at the center of the crossing, the theoretical curves for interaction ratios

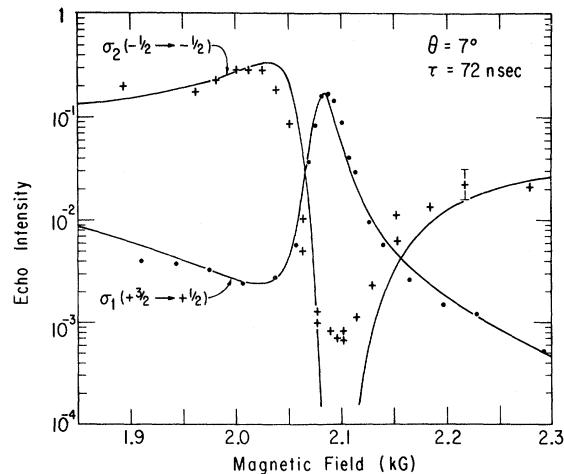


FIG. 7. Photon-echo intensity as a function of magnetic field near the 2.06-kG level crossing for the $\sigma_1(+\frac{3}{2} \rightarrow +\frac{1}{2})$ and $\sigma_2(-\frac{1}{2} \rightarrow -\frac{1}{2})$ transitions. The magnetic field angle θ is 7° and the pulse separation time 72 nsec. Data points are from Ref. 16 and the curves from our theory.

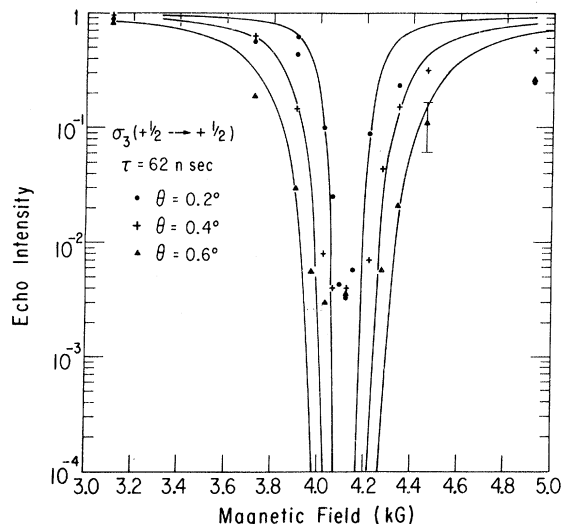


FIG. 8. Photon-echo intensity data as a function of magnetic field near the 4.12-kG level crossing for the $\sigma_3(+\frac{1}{2} \rightarrow +\frac{1}{2})$ transition for various angles θ of magnetic field with the corresponding theoretical curves. The pulse separation time is 62 nsec.

of 1.0 predict the echo behavior quite well. As shown in the figure, the level crossing at 4 kG has a very sharp angular magnetic field dependence. This is a result of the fact that as the applied magnetic field is aligned closer to the optic axis of the crystal, the range of magnetic fields for which there is appreciable mixing of the $+\frac{1}{2}$ and $+\frac{3}{2}$ states decreases rapidly. This effect is particularly useful experimentally, since it allows the crystal to be aligned accurately with the magnetic field, i. e., within 0.1° . This ability to make precision alignments of the magnetic field is important for angular dependence and on-axis decay measurements.

E. Zero-Field Echo

We have calculated the photon-echo-decay curves for the zero-field case. When there is no external field the local magnetic field at the Cr site, due to all the other Cr spins and Al nuclei, must be included in the calculation. Our calculations indicate that the magnitudes of these small local fields are relatively unimportant; however, the directions of these fields are very important since they determine the initial orientation of the ground-state Cr spin. We have calculated the zero-field decay by assuming a local field of 5 G which has a uniform spherical distribution of field orientations. By calculating the decay amplitude for various angles between the field and the optic axis and taking the appropriate weighted average for a spherical distribution, we obtain the rapid echo decay shown in Fig. 9. This decay is in agreement with early

experiments which showed that the zero-field echo can only be observed for short pulse separation times.²³ Our experimental points (Fig. 9) confirm that the zero-field echo can only be observed at short times; however, experimental difficulties in obtaining low fields with our apparatus resulted in rather large error limits on our zero-field data. Thus we have been able to show only rough agreement between theory and experiment at low fields. It should be observed, however, that both the experimental points and the theory indicate a rapid decay of the zero-field photon echo for pulse separation times in excess of 40 nsec. This implies that ruby cannot be treated as a simple two-level system for times long enough for interference to occur. The failure of the two-level approximation may have important consequences in self-induced-transparency²⁴ experiments when the pulse width or pulse delay exceeds 40 nsec. Of course, as we stated earlier, ruby approximates a two-level system when a magnetic field of a few kilogauss is applied parallel to the optic axis.

F. Other Results

There are a few other results which deserve comment. First, with regard to the Al modulation effect in more concentrated ruby, the modulations are unaffected by Cr concentration except that the

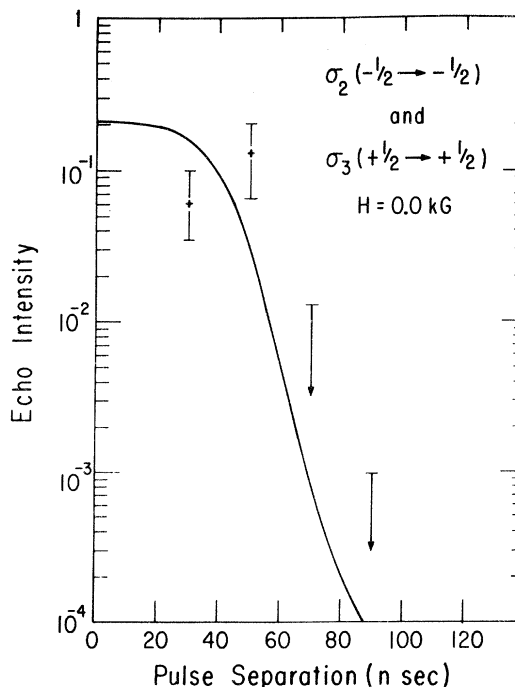


FIG. 9. Calculated photon-echo decay at zero magnetic field for the $\sigma_2(-\frac{1}{2} \rightarrow -\frac{1}{2})$ and $\sigma_3(+\frac{1}{2} \rightarrow +\frac{1}{2})$ transitions. The decays for both transitions are identical at zero field. For $\tau > 50$ nsec the experimental echo signal is given as an upper limit only.

level crossings are broadened due to the increased magnetic linewidths in the crystal. This broadening of the level crossings was reported previously,²⁵ although not explained on the basis of Cr-Al interactions. There are other effects at the level-crossing fields in concentrated ruby which arise from Cr-Cr interactions,²⁶ such as the appearance of dips in the echo signal for the noncrossing states. The contribution of the Cr-Cr interaction to the level crossings has been studied in detail, both experimentally and theoretically, by Compaan.¹ Finally, since the Al nuclei have a quadrupole moment, there are level crossings in the Al eigenstates. If these level crossings affected the photon echo in any observable way, one would have a very precise way of measuring the excited-state interactions. A computer simulation of an echo versus magnetic field experiment was done to check this possibility and found that within the framework of the present theory there is no observable effect of the nuclear level crossings on the photon echo.

V. FLUORESCENCE-LINEWIDTH CALCULATIONS

The homogeneous optical linewidth in ruby has been observed recently by Szabo¹⁷ using a laser-induced fluorescent-line-narrowing technique. Szabo suggests that the observed linewidths are due to the superhyperfine interactions²⁷ between Cr and the 13 nearest-neighbor Al nuclear spins. Equation (12) predicts the time-dependent fluorescence due to the Al neighbors following pulsed excitation. From Eq. (12) the contribution to the homogeneous linewidth can be calculated by taking the Fourier transform of the fluorescence-decay curve numerically. We have calculated the homogeneous linewidth contributions for the magnetic fields and transitions studied by Szabo. The full width at half-maximum (FWHM) for a 420-G field at 0° is calculated to be 0.7 MHz for the σ_2 transition, 0.9 MHz for the σ_3 transition, and 20 MHz for the σ_1 transition. With a magnetic field of 140 G at 90° the calculated widths are 19 MHz for σ_1 and 25 MHz for σ_2 . The calculated widths for the 0° cases appear to be consistent with Szabo's recent data²⁸ for 0.01 wt% ruby which show that the ${}^4A(\pm\frac{1}{2})$ to ${}^2E(\pm\frac{1}{2})$ transitions have a linewidth less than the 12-MHz instrumental resolution, while the ${}^4A(\pm\frac{3}{2})$ to ${}^2E(\pm\frac{3}{2})$ transitions have an experimental width of 35 ± 5 MHz. In the 90° field case, Szabo measures widths of about 100 MHz for all lines, while our calculations give widths of 19 and 25 MHz. We do not expect exact agreement between widths predicted for broad-band (pulsed) excitation and those measured using narrow-band (cw) excitation as in Szabo's experiments. We consider the predicted qualitative features of the magnetic field properties and the widths for the 0° cases to be in good agreement

with present data. The narrower calculated widths in the 90° field case may indicate the presence of other homogeneous broadening mechanisms.

All the calculations we have done show that photon-echo decays and fluorescence decays have qualitatively similar magnetic field properties. Thus we expect that fluorescence-linewidth experiments will reveal effects which can be correlated with photon-echo behavior. For example, whenever the photon-echo decay is rapid there should be a correspondingly broad fluorescence line as is the case for 90° fields. Likewise, a slow photon-echo decay would indicate a narrow fluorescence line as is the case for high magnetic fields at 0°. For cases where there is a strong modulation of the echo, the fluorescence spectrum may have side bands at the modulation frequency. Level crossings could also prove to be very interesting in the fluorescence spectrum. We expect that the σ_2 and σ_3 transitions will have broader lines at their respective level crossings, whereas the σ_1 transition should have a narrower line at the crossing.

VI. CONCLUSION

It has been demonstrated experimentally that most of the concentration- and temperature-independent properties of the photon echo in ruby are the consequence of the radiative interference of coherently excited multiplets of energy levels arising from the superhyperfine interaction of the Cr spin with the 13 nearest-neighbor Al nuclei. With the exception of a slightly enhanced on-axis decay in very dilute ruby (0.006 wt%) all the known temperature-independent properties of the photon echo in ruby can be explained either by the theory presented here or by the Cr-Cr spin interactions discussed by Compaan.¹ In particular our calculations based on the superhyperfine interactions are in quantitative agreement with the observed spin dependence of the echo decay, the modulation of the echo intensity as a function of pulse separation time, the details of the echo behavior at the level crossings (most notably the increase in the σ_1 echo intensity at 2.06 kG), the echo-intensity dependence on the direction and magnitude of an applied magnetic field, as well as the rapid decay in zero field. The 2E excited-state contact interaction strengths which best fit our data are approximately the same as the corresponding contact interactions for the 4A_2 state. With the excited-state interaction parameters determined here, we have calculated from our theory of fluorescence decay the fluorescence-linewidth contribution of the near-neighbor Al nuclei and obtain agreement with recent measurements.¹³ Furthermore, the theory demonstrates an intimate relationship between photon-echo behavior, fluorescence modulation, and line spectra.

ACKNOWLEDGMENTS

The support and encouragement of Professor I. D. Abella through all phases of this research is

gratefully acknowledged. I also gratefully appreciate the many helpful comments and invaluable assistance of Dr. A. Compaan, and the laboratory assistance of C. Y. Pang and S. Paranjape.

*Work supported in part by the National Science Foundation under Grant No. GP-18622, and in part by the Advanced Research Projects Agency Contract No. DAHC 15-67-C-0220.

¹Submitted as a thesis to the Department of Physics, The University of Chicago, in partial fulfillment of the requirements for the Ph.D. degree.

¹A. Compaan, Phys. Rev. B **5**, 4450 (1972).

²L. Q. Lambert, A. Compaan, and I. D. Abella, Phys. Rev. A **4**, 2022 (1971).

³I. D. Abella, N. A. Kurnit, and S. R. Hartmann, Phys. Rev. **141**, 391 (1966).

⁴M. O. Scully, M. J. Stephen, and D. C. Burnham, Phys. Rev. **171**, 213 (1968); R. G. Brewer and R. L. Shoemaker, Phys. Rev. Lett. **27**, 633 (1971); A. I. Alekseev and I. V. Evseev, Zh. Eksp. Teor. Fiz. **57**, 1735 (1969) [Sov. Phys.-JETP **30**, 938 (1970)]; V. V. Samartsev and V. R. Nagibarov, Fiz. Tverd. Tela **11**, 3669 (1969) [Sov. Phys.-Solid State **11**, 3085 (1970)].

⁵J. P. Gordon, C. H. Wang, C. K. N. Patel, R. E. Slusher, and W. J. Tomlinson, Phys. Rev. **179**, 294 (1969).

⁶D. Grischkowsky and S. R. Hartmann, Phys. Rev. B **2**, 60 (1970).

⁷L. G. Rowan, E. L. Hahn, and W. B. Mims, Phys. Rev. A **137**, 61 (1965).

⁸N. A. Kurnit, I. D. Abella, and S. R. Hartmann, Phys. Rev. Lett. **13**, 567 (1964).

⁹A. Compaan, L. Q. Lambert, and I. D. Abella, Phys. Rev. Lett. **20**, 1089 (1968).

¹⁰L. Q. Lambert, A. Compaan, and I. D. Abella, Phys. Lett. A **30**, 153 (1969).

¹¹J. Macek, Phys. Rev. Lett. **23**, 1 (1969); G. W. Series, Physica (Utr.) **33**, 138 (1967), and references therein.

¹²H. J. Andra, Phys. Rev. Lett. **25**, 325 (1970).

¹³T. Hadeishi and W. A. Nierenberg, Phys. Rev. Lett. **14**, 891 (1965).

¹⁴J. N. Dodd, R. D. Kaul, and D. M. Warrington, Proc. Phys. Soc. Lond. **84**, 176 (1964); E. B. Aleksandrov, Opt. Spektrosk.

17, 957 (1964) [Opt. Spectrosc. **17**, 522 (1964)]; J. N. Dodd, W. J. Sandle, and D. Zissermann, Proc. Phys. Soc. Lond. **92**, 497 (1967).

¹⁵D. A. Jensen, S. H. Aronson, R. D. Ehrlich, D. Fryberger, C. Nissim-Sabat, V. L. Telegdi, H. Goldberg, and J. Solomon, Phys. Rev. Lett. **23**, 615 (1969).

¹⁶A. Compaan, L. Q. Lambert, and I. D. Abella, Opt. Commun. **3**, 236 (1971).

¹⁷A. Szabo, Phys. Rev. Lett. **27**, 323 (1971); **25**, 924 (1970).

¹⁸E. O. Schulz-duBois, Bell Syst. Tech. J. **38**, 271 (1959).

¹⁹N. Laurance, E. C. McIrvine, and J. Lambe, J. Phys. Chem. Solids **23**, 515 (1962).

²⁰J. U. White, J. Opt. Soc. Am. **32**, 285 (1942).

²¹P. F. Liao and S. R. Hartmann, Phys. Lett. A **38**, 295 (1972).

We have tested the theoretical fit using the remeasured quadrupole constants and found that in most cases the curves are indistinguishable. Figure 3 shows the effects of the small change of quadrupole constant in the most sensitive region.

²²R. V. Pound, Phys. Rev. **79**, 685 (1950).

²³N. A. Kurnit and S. R. Hartmann, *Interaction of Radiation with Solids* (Plenum, New York, 1967), p. 693; I. D. Abella, in *Progress in Optics*, edited by E. Wolf (North-Holland, Amsterdam, 1969), Vol. VII, p. 158.

²⁴S. L. McCall and E. L. Hahn, Phys. Rev. Lett. **18**, 908 (1967); Phys. Rev. **183**, 457 (1969); C. K. N. Patel and R. E. Slusher, Phys. Rev. Lett. **19**, 1019 (1967); I. M. Asher and M. O. Scully, Opt. Commun. **3**, 395 (1971); I. M. Asher, Phys. Rev. A **5**, 349 (1972).

²⁵L. Q. Lambert, A. Compaan, and I. D. Abella, Bull. Am. Phys. Soc. **15**, 88 (1970).

²⁶A. Compaan and I. D. Abella, Bull. Am. Phys. Soc. **16**, 1403 (1971).

²⁷R. F. Wenzel, Phys. Rev. B **1**, 3109 (1970).

²⁸A. Szabo, in Proceedings of the Seventh International Quantum Electronics Conference, Paper I-8, Digest of Technical Papers, 1972 (unpublished), p. 44; and private communication.

Strong-Field Assignment on $4f^{13} 5d$ Levels of Yb^{2+} in SrCl_2

Eugene Loh*

Laboratoire de Chimie Physique "Matière et Rayonnement" Associé au, Centre National de la Recherche Scientifique, Université de Paris VI, 75 005-Paris-France
(Received 11 September 1972)

The $4f^{14} \rightarrow 4f^{13} 5d$ absorption spectrum of an Yb^{2+} ion in cubic crystals is demonstrated to have four peaks, which correspond to the four $5d$ (e_g or t_{2g}) $4f^{13}$ (${}^2F_{7/2}$ or ${}^2F_{5/2}$) final states.

The $4f^{n-1} 5d$ configuration of most of the divalent and trivalent rare-earth ions in solids is known^{1,2} to be formed by weak interaction between the $5d$ orbitals, which are split strongly in the crystal field, with the $4f^{n-1}$ core. For example, the $4f^{14} \rightarrow 4f^{13} 5d$ absorption spectrum³ of Yb^{2+} in CaF_2 con-

sists of e_g and t_{2g} components of the $5d$ electron with a separation of 16700 cm^{-1} . Each of these $5d$ orbitals has a high-energy partner,³ which corresponds to the ${}^2F_{7/2} \rightarrow {}^2F_{5/2}$ transition of Yb^{3+} ($4f^{13}$) at $\sim 10000 \text{ cm}^{-1}$. For each Yb^{2+} ion in the cubic crystal there are therefore four $4f^{14} \rightarrow 4f^{13} 5d$ ab-